European Journal of Mechanics B/Fluids 55 (2016) 294–299

Contents lists available at ScienceDirect

European Journal of Mechanics B/Fluids

journal homepage: www.elsevier.com/locate/ejmflu

Turbulence modification by dispersion of large deformable droplets☆

Luca Scarbolo [a], Federico Bianco [a], Alfredo Soldati [a,b,*]

[a] Department of Elec., Manag. and Mechanical Engineering, University of Udine, 33100, Udine, Italy

[b] Department of Fluid Mechanics, CISM, 33100, Udine, Italy

ARTICLE INFO

Article history:
Available online 1 November 2015

Keywords:
Droplets
Coalescence
Breakup
Turbulence
Phase field
Direct numerical simulation

ABSTRACT

Dispersion of large deformable droplets in turbulent channel flow is investigated: the fluids are considered of same density and viscosity for a broad range of plausible values of surface tension. Droplets much larger than the Kolmogorov length scale are released in a channel flow; the turbulent flow is computed with pseudo-spectral Direct Numerical Simulations (DNS), while phase interactions are described with a Phase Field Model (PFM). It is shown that droplets segregation toward the center of the channel is promoted by deformability in particular, for the considered Weber numbers (ratio between inertia and surface tension), droplets do not deposit on the walls. The turbulent flow is modified by the presence of the droplets: for small values of *We* the wall drag is increased with respect to the single phase flow. The wall drag enhancement reduces increasing *We* and its time evolution depends on the droplets coalescence and breakup rates.

1. Introduction

Two-phase flows where large deformable droplets are dispersed in turbulent wall bounded flows are encountered in many industrial applications; the turbulent water–oil emulsions obtained from the water lift of the crude oil are an important example of these flows. In these two-phase flows, the dispersed phase is subjected to complex phenomena like deformations, breakups or coalescence; moreover the presence of a dispersed phase can heavily affect the motion of the carrier phase due to the large relative velocities at the droplets interface. In the simplest configuration, the fluid system is constituted by two immiscible and incompressible pure components whose interfaces are endowed by surface tension; although being simplified, the physical system is still dominated by complex phenomena: droplets turbulent dispersion, droplet–droplet interactions and wall-drag modifications. Objective of this work is to investigate the dispersion of a swarm of neutrally buoyant droplets in a turbulent channel flow at various values of the surface tension (here represented by the Weber number), focusing on the droplets segregation and on the wall-drag modifications. In order to further simplify the problem and reduce the number of experiments necessary to completely describe the actual physical system, droplets and continuous phase are considered as density and viscosity matched. In view of this strong simplification, the results of this work can be considered as the limit case of heavy droplets where inertia effects are dominant. Droplets are large compared to the smallest turbulent scale and they can deform, break and coalesce. The investigation is performed through the Phase Field Model (PFM) [1–4], a robust and accurate numerical framework tailored for the description of turbulent multiphase flows that has shown promising capabilities in the analysis of deformable breaking and coalescing fluid–fluid interfaces [5–7]. In particular the PFM can be easily extended to cases of strong viscosity ratios [5], while the description of density mismatch is possible adopting a density based formulation of the model.

The problem of wall-drag modification produced by large droplets in turbulent wall-bounded flow has been tackled by the authors in a previous work [8] where the average effect of the droplets on the wall drag has been analyzed and correlated to the vorticity fluctuations. By contrast this work focuses on the time evolution of the wall-drag modifications and their correlation to the droplets dispersion, coalescence and breakup. To the authors' knowledge, this work represents one of the first computational efforts toward the study of the collective dynamics of large deformable droplets in turbulent wall-bounded flows. While many

☆ It is our great pleasure to take part in this Festschrift Issue dedicated to Professor Paolo Orlandi on the occasion of his 70th birthday. Buon compleanno Paolo! We wish you many more fruitful and happy years with the same enthusiasm for science and knowledge you always had.

* Corresponding author at: Department of Elec., Manag. and Mechanical Engineering, University of Udine, 33100, Udine, Italy.

E-mail addresses: luca.scarbolo@ge.com (L. Scarbolo), soldati@uniud.it (A. Soldati).

http://dx.doi.org/10.1016/j.euromechflu.2015.10.002
0997-7546/

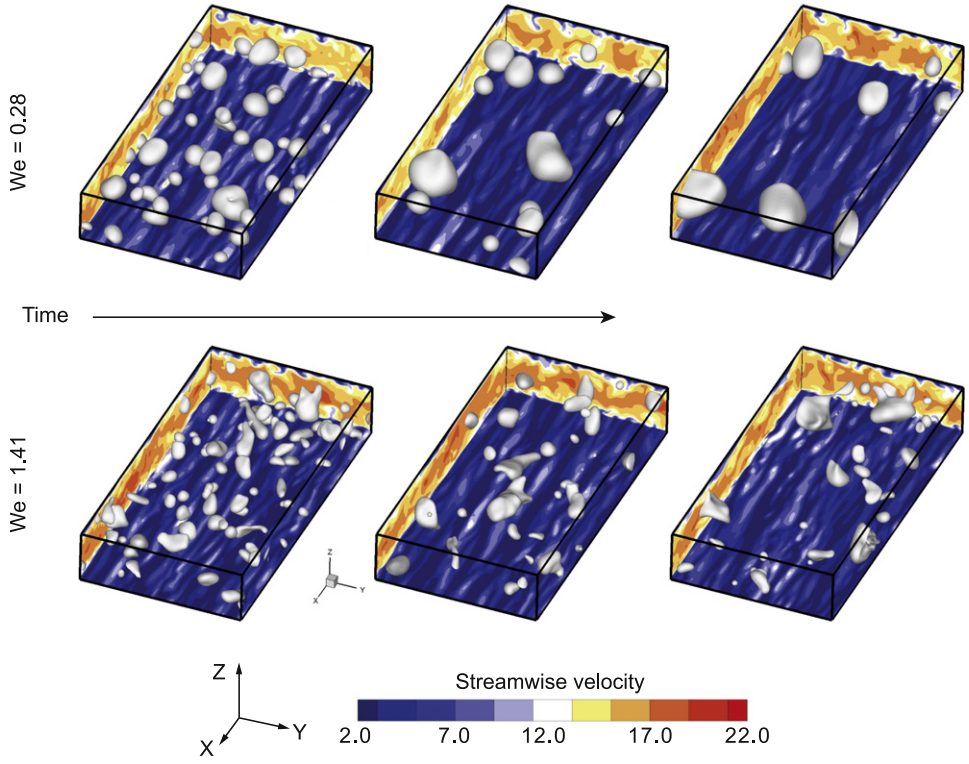

Fig. 1. Droplets evolution in channel flow for two different Weber numbers (upper and lower panel row). Streamwise velocity u is rendered on xy, xz and yz slices.

authors focused on the dispersion of point-wise particles in turbulent flows and their effects on the wall drag, only few examples of finite size droplets or bubbles dispersion in turbulence can be found. Some authors focused on the preferential segregation of finite size rigid particles in laminar flows [9,10], while similar phenomena have been observed and studied experimentally in moderate turbulence [11]. Very few investigations of the dispersion of large deformable droplets and bubbles in turbulence can be found: the segregation and modifications of turbulence regeneration mechanisms produced by the dispersion of large bubbles in wall-bounded turbulence have been approached neglecting the simulation of relevant effects such as breakup and coalescence [12]. By contrast, other works focused on the coalescence and fragmentation of interfaces in isotropic turbulence [13,14].

2. Physical problem and modeling

A swarm of $n_{d,0}$ droplets of initial diameter d_0 has been released in a fully developed turbulent channel flow; the two fluid phases (dispersed and continuous phase) have the same density $\rho_f = \rho_d = \rho$ and the same kinematic viscosity $\nu_f = \nu_d = \nu$ (subscripts f and d stand for continuous phase flow and dispersed phase, respectively). The two fluids are considered immiscible, incompressible and Newtonian, moreover their interface is endowed with surface tension. In spite of being largely simplified, the resulting physical system retains the most important features of the problem: the turbulent motion and the momentum transfer between the phases are described in great detail. The problem is described by the following dimensionless governing equations solved on a channel of size is $4\pi H \times 2\pi H \times 2H$ in streamwise (x), spanwise (y) and wall-normal (z) directions, respectively (Fig. 1).

$$\nabla \cdot \mathbf{u} = 0, \tag{1}$$

$$\frac{\partial \mathbf{u}}{\partial t} = -\mathbf{u} \cdot \nabla \mathbf{u} - \nabla p - \nabla \Pi + \frac{1}{Re_\tau} \nabla^2 \mathbf{u} + \frac{3}{\sqrt{8}} \frac{1}{We \cdot Ch} \mu \nabla \phi, \tag{2}$$

$$\frac{\partial \phi}{\partial t} = -\mathbf{u} \cdot \nabla \phi + \frac{1}{Pe} \nabla^2 \mu, \tag{3}$$

$$\mathcal{F}(\phi) = f(\phi) - Ch^2 |\nabla \phi|^2 = \frac{1}{4} (\phi - 1)^2 (\phi + 1)^2 - Ch^2 |\nabla \phi|^2, \tag{4}$$

$$\mu = \frac{\delta \mathcal{F}}{\delta \phi} = \phi^3 - \phi - Ch^2 \nabla^2 \phi. \tag{5}$$

Eqs. (1)–(2) are the incompressible Navier–Stokes equations, where $\mathbf{u}$ is the incompressible velocity field and p and Π are the fluctuating and mean components of the pressure field, respectively. Eq. (3) is the phase field conservation equation, known as Cahn–Hilliard equation; in the PFM framework the two components are described as a mixture through a continuous scalar order parameter $\phi(\mathbf{x})$. The order parameter assumes constant values ϕ_+ and ϕ_- in the bulk fluid regions and it is characterized by smooth variations across the fluid–fluid interface. The thermodynamic chemical potential, μ, describes the variation of free energy ($\mathcal{F}(\phi)$) resulting from a small local change of composition of the mixture; the free energy $\mathcal{F}(\phi)$, (4), is the sum of a double-well potential $f(\phi)$ (that keeps in account the phobic behavior) and a non-local term ($Ch^2|\nabla\phi|^2$) that accounts for the non zero surface tension. Due to surface tension, Eqs. (2) and (3) are coupled via the capillary force term, $\frac{3}{\sqrt{8}} \frac{1}{We \cdot Ch} \mu \nabla \phi$, that describes the momentum exchanged between the two fluids at the interface. Eqs. (1)–(5) are rewritten in a non-dimensional formulation using the scaling quantities U_τ, H and ϕ_+, where $U_\tau = \sqrt{\tau_w/\rho}$ is the shear velocity based on the wall shear stress τ_w and the fluid density ρ. The non-dimensional groups that appear in Eqs. (1)–(4) are defined as follows:

$$Re_\tau = \frac{U_\tau H}{\nu}, \qquad Pe = \frac{U_\tau H}{M}, \qquad We = \frac{\rho U_\tau^2 H}{\sigma}, \qquad Ch = \frac{\xi}{H}, \tag{6}$$

where M is the fluid mobility inside the interfacial layer of thickness ξ and surface tension σ. The shear Reynolds number (Re_τ) is the ratio between inertial forces and viscous forces and the Weber

number (We) is the ratio between inertial forces and the surface tension. In the PFM the Peclet number (Pe) represents the ratio between the diffusive time scale H^2/M and the convective time scale $H/(U_\tau H)$ in the interfacial layer and it controls the interface characteristic relaxation time; the Cahn number (Ch) is the dimensionless interface thickness (or capillary width).

In this work, Re_τ and We are input parameters that are defined by considering the physical properties of the fluids, the flow regime and the surface tension; furthermore the flow is driven by imposing a mean pressure gradient $\nabla \Pi$ along the streamwise direction. Once the shear Reynolds number is fixed, the value of the surface tension is chosen by changing the Weber number. The PFM here adopted is based on a thermodynamic framework that is rigorous when simulating near critical systems, namely mixtures where the interface thickness is a transition layer of the same order of the problem length scale $Ch \propto O(H)$ [3,2]. When considering mixtures of fluids far from critical point, the physical interface thickness is extremely small, of the order of molecular length-scale [15,16], therefore $Ch \to 0$. The numerical resolution of such interface thickness is beyond the current computational limits (and beyond the continuum hypotheses, as well) thus, for a given spatial discretization, Ch is chosen as the smallest value that guarantees a good (spectral) numerical accuracy [5]. Once the Cahn number is fixed, a consistent 'sharp-interface limit' ($Ch \to 0$) is recovered imposing $Pe \propto Ch^{-1}$. As shown by means of formal asymptotic expansions [4], in such limit, the Cahn–Hilliard equation (3) describes the advection of the order parameter ϕ, preventing the degradation of the interface profile and granting higher accuracy with respect to Level-Set methods. As a result the value of surface tension σ is correctly represented and the capillary force coupling term in the Navier–Stokes equations (1)–(2) is equivalent to any continuum surface force (CSF) formulation [17].

2.1. Simulation parameters

The equations system (1)–(5) has been solved using a pseudo-spectral approach [18] where periodic boundary conditions have been applied along the homogeneous streamwise and spanwise directions (x and y) for both velocity field and order parameter; no-slip velocity and normal contact angle for the interface have been imposed at the walls [19,5]. An initial number of $n_{d,0} = 256$ droplets of diameter $d = 0.6$ (non dimensionalized with the channel half height H) have been initialized superposing the scalar field ϕ over a fully developed turbulent flow obtained from previous single phase simulations; the volume fraction of the droplets is $\varphi = 0.054$. Since the two fluids are density and viscosity matched the initial transient is extremely fast. In order to consider a fully developed turbulent flow, the shear Reynolds number is set $Re_\tau = 150$; in this regime the initial droplet diameter is much larger than the Kolmogorov length scale η_κ and the ratio between the Kolmogorov length scale and the droplet diameter is $0.027 \leq \eta_\kappa/d_0 \leq 0.063$. The simulations have been performed considering a wide range of Weber numbers: $We = 0.18 \div 2.8$. The values have been selected first considering typical values of density, viscosity and surface tension of a light crude oil (respectively: $\rho = 058$ kg/m^3, $\nu = 6 \cdot 10^{-6}$ m^2/s and $\sigma = 0.025$ N/m) flowing in a channel of $H = 0.02$ m ($We \simeq 1.6$). The range has been extended toward smaller and higher values of Weber numbers to investigate the effects of surface tension limiting We to values at which wall-drag modifications are significative. Simulations were run on a $512 \times 256 \times 257$ fixed Cartesian grid fine enough to resolve the smallest length scale of the turbulent flow: uniform spacing $\Delta x = \Delta y = 0.245$ is imposed along the stream-wise and the span-wise directions, while a non uniform (Chebyshev based) nodes distribution is applied along the wall-normal direction. The time step $\Delta t = 10^{-4}$ has been chosen to resolve the smallest temporal scales and respond to the numerical stability requirements associated with the grid resolution. With the chosen grid size and the required time step constraint, the present simulations required almost $2 \cdot 10^6$ CPU-hours on a large parallel HPC infrastructure, producing $3TB$ of raw computational data. The pseudo-spectral scheme adopted can resolve accurately the interfacial layer with a minimum number of three mesh-points [5,20]. Here the interface is described by three mesh-points along x and y directions (where a uniform discretization is adopted) and by a minimum number of seven mesh-points along the z direction where a finer non-uniform discretization is adopted (Chebyshev polynomials). With the grid resolution adopted, the interface thickness (a layer where $-0.9 \leq \phi \leq 0.9$) is fixed choosing $Ch = 0.0185$ and, according to the scaling law [4], the Peclet number is $Pe = 162.2$. The interface thickness is larger than the Kolmogorov length scale $0.36 \leq \eta_\kappa/Ch \leq 0.84$, thus the interface cannot be deformed by eddies of that size. This drawback is unavoidable when smearing the interfacial forces over a finite thickness layer, thus it afflicts all the CSF methods; however the size of the damped eddies is in any case small compared to the droplet diameter. The PFM cannot completely fulfill local mass conservation [6,20]; thanks to the accuracy of the numerical and to the small interface thickness adopted, however, the mass loss is in any case small.[1]

3. Results and discussion

In order to highlight possible mid-channel segregation, droplets are released in an equally spaced arrangement in the near wall regions. Droplets center of mass is set at a distance $z^+ = 54w.u.$ From each wall superposing the scalar field ϕ over a turbulent velocity field obtained from previous fully developed single phase simulations. The time needed for the flow to adapt to the superposition of the scalar field ϕ, is extremely short: namely only the capillary forces at the droplets interfaces need to be balanced and the choice of Pe ensures an interface relaxation time much faster than the time scale of the external convective forcing [20,8]. As a result, settling of the initial interface profile are almost immediate. After being released, droplets are advected by the flow stream and three distinct phenomena that can be observed for the transport dynamics: (i) droplet interface modifications; (ii) droplets segregation; (iii) wall drag modifications. In this work only droplets segregation and wall drag modifications will be considered. The complex droplet interface modifications can be briefly summarized in the following way: for small Weber numbers ($We < 1$ in the present work) droplet coalescence dominates until geometric separation prevents the phenomena, leading to a We independent asymptotic number of droplets; for large Weber numbers ($We > 1$) inertial forces are strong enough to produce the breakup of droplets larger than a critical diameter [21], resulting in a persistent dynamic balance between coalescence and breakup [7].

3.1. Droplets segregation

It is known [9,10] that a swarm of neutrally buoyant rigid particles, uniformly released in a laminar pipe flow, tend to accumulate on a narrow annulus. This inertia driven phenomena, originally known as tubular pinch, was first observed at low

[1] After the entire simulation ($2 \cdot 10^5$ time-steps, corresponding to ~50 channel length covered by the mean flow), losses of volume V^- (or equivalently of mass m) range from 2% to 10%.

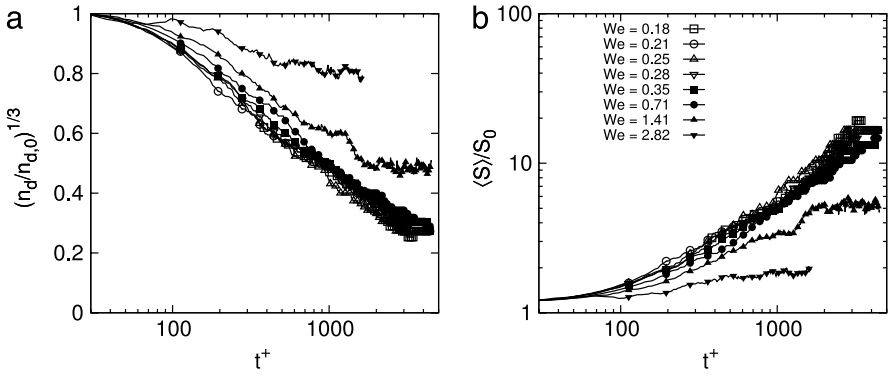

Fig. 2. Time evolution of the collective surface area $S_t \propto (n_d/n_{d,0})^{1/3}$ (panel a) and normalized mean droplet surface $\langle S\rangle/S_0$ (panel b) as function of the Weber number *We*.

Reynolds number flows for relatively large particles ($d/D = 8 - 42$ being d and D particle and pipe diameter). When moving to turbulent flows, the radial segregation phenomena is blurred by the turbulent mixing; nevertheless it has been experimentally observed that radial preferential concentration still persists for rigid particles of diameter $d/D = 17$ in moderate turbulent flows up to $Re = 2400$ [11].

In the case of deformable light dispersed phase (bubbles), numerical investigations [12] have shown that deformability plays a central role in the bubbles segregation. In fact, non-deformable bubbles tend to accumulate near the wall and deposit, while deformable bubbles are pushed in the center of the channel avoiding walls showing, in fact, a segregation in the center of the channel.

In this case, the neutrally buoyant and deformable droplets in a moderate turbulent flow ($Re_\tau = 150$) show clear Weber dependent segregation toward the channel center. In Fig. 3 the volume fraction profile α is reported at different times: the turbulent advection produces a spatial redistribution of the dispersed phase, qualitatively ruling out the initial distribution shows after $1200t^+$. For the complete range of Weber number here considered, the dispersed phase accumulate always at the center of the channel: in agreement with results obtained for deformable bubbles [12], larger deformability enhances this droplets segregation. Due to the non uniform wall-normal flow distribution the droplets are driven toward the center of the channel: the droplets tend to move toward regions of smaller shear [9,10], and the observed phenomena is opposite to the segregation driven by the lift forces in the case of micro bubbles dispersion [22,23]. Moreover, due to the droplets size, entrainment in the near wall region ($z^+ < 15$) is probably not possible even releasing the droplets closer to the wall; nevertheless a complete investigation of the segregation leading mechanisms is out of the bounds of the present work. Droplets never deposit on the walls, despite this mechanism has not been artificially prevented through the numerical setup: the boundary conditions adopted yield to a normal contact angle at the walls. Nevertheless, large droplets, for the whole range of deformability, tend to avoid impacts with the walls. In addition, Fig. 3 (panels d–h) shows that less deformable droplets (small *We*) can reach smaller distances from the walls suggesting that wall impact and deposition is likely to be observed at smaller *We*. Authors have observed deposition of droplets and thin film formation at the walls, for $We = 0.014$ (simulation that has been performed but not reported in this work).

3.2. Dynamics of the carrier phase

The presence of a dispersed phase is affecting the features of the turbulent flow: depending on the Weber number, the droplets can promote or reduce the momentum transfer between fluid regions at diameter distance: $l \sim d$. When the turbulent forcing is weaker than the surface tension σ, here $We < 1$, the droplets can efficiently affect the local turbulent structures while, when the turbulent forcing is larger than σ, the capillary forces at the droplets interface produce small modifications of the local flow field and the fragmentation mentioned in Section 3 can be observed [7]. To quantify the impact of the droplets on the flow field, the instantaneous friction coefficient is defined as:

$$C_f = \frac{\nabla \Pi}{\frac{1}{2}\rho u_b^2}, \tag{7}$$

where $\nabla\Pi$ is the mean pressure gradient that is driving the flow and u_b is the instantaneous bulk velocity. In the case of a single phase turbulent flow, C_f is constant and equal to $C_{f,s}$. After the droplets injection the transported phase starts to interact with the turbulent structures, resulting in a variation of C_f. Since the driving force is kept constant in the simulations, variation of the friction coefficient is due to variation of the flow rate only. The time evolution of the friction coefficient normalized with the average single-phase friction coefficient $C_{f,s}$, is reported in Fig. 4(a). As expected, C_f depends on the Weber number: when the surface tension is smaller than the turbulence forcing ($We < 1$) almost negligible modifications of C_f are observed; by contrast, decreasing *We*, increments of C_f (and consequently of the wall-drag) are observed. When $We < 1$, the friction coefficient is characterized by a non monotonic behavior: (i) C_f increases up to $t^+ \simeq 1000$; (ii) a almost steady condition is maintained when $1000 \leq t^+ \leq 2000$; (iii) C_f reduces when $t^+ \geq 2000$. This wall-drag reduction is in any case small and needs a detailed investigation of the possible physical phenomena underpinning it. One of the possible explanations is through the vorticity modification mechanism [12]: due to the high shear present in the near wall region, droplets are forced to move at a favorable wall-distance to sustain the canceling of the local vorticity fluctuations. Clearly this has to be supported by the measurements of vorticity that are out of the scope of this paper. The non monotonic behavior of C_f can be explained considering two factors: (i) the droplets can exchange forces through their external surface, only; (ii) the flow field modifications are mainly due to the streamwise velocities differences experienced by the droplet, due to its finite size. Due to droplets coalescence, the total surface area of the swarm of droplets can be roughly estimated as $S(t) \sim n_d^{1/3}$, thus it reduces in time according to the time evolution of the droplet swarm (Fig. 2(a)).

At the same time, due to the average diameter increment, the average surface of the single droplet $\langle S\rangle$ increases (Fig. 2(b)). The velocity difference Δu experienced by the droplets is larger the larger is the droplet diameter, in fact larger size bodies can span wider regions in the non homogeneous wall-normal direction. As a result, the behavior of C_f can be considered as the effect of the velocity difference Δu that increases in time, modulated by

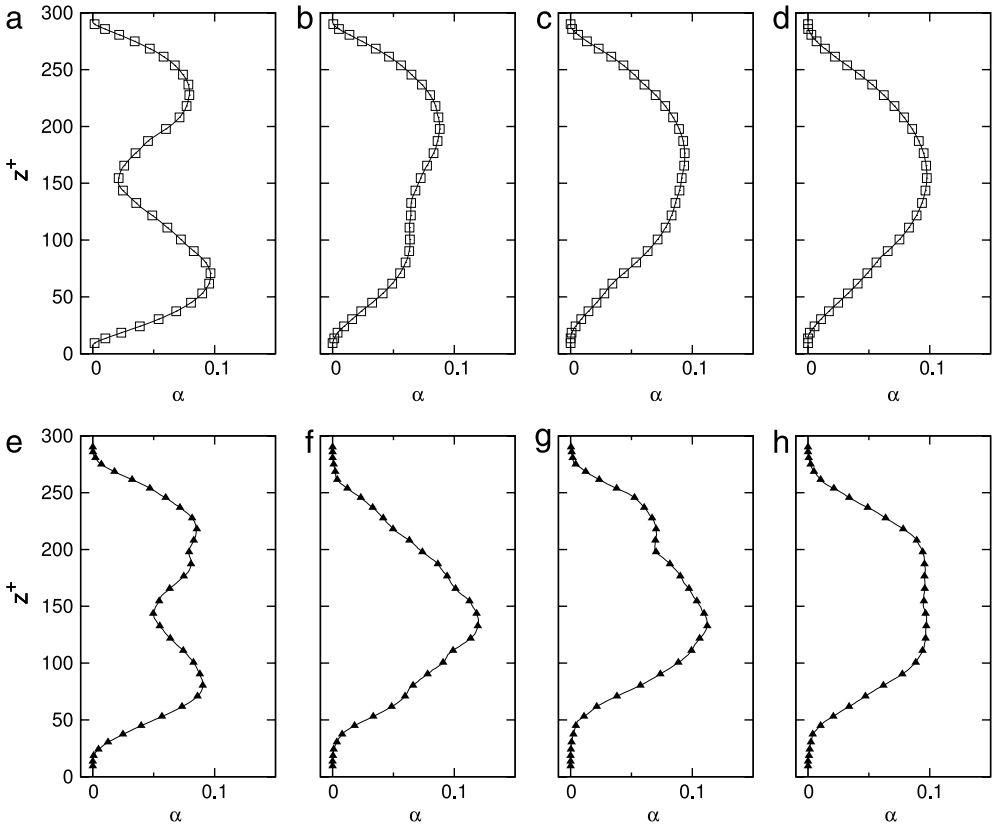

Fig. 3. Distribution of the dispersed phase volume fraction α along the channel height z. Two different Weber numbers are shown: $We = 0.28$ in the top panels (a)–(d), $We = 1.41$ in the bottom panels (e)–(h). Different simulation times are considered: $t^+ = 600$ for panels (a) and (e); $t^+ = 1350$ for panels (b) and (f); $t^+ = 2100$ for panels (c) and (g); $t^+ = 2850$ for panels (d) and (h). The same Weber numbers times are shown in Fig. 1.

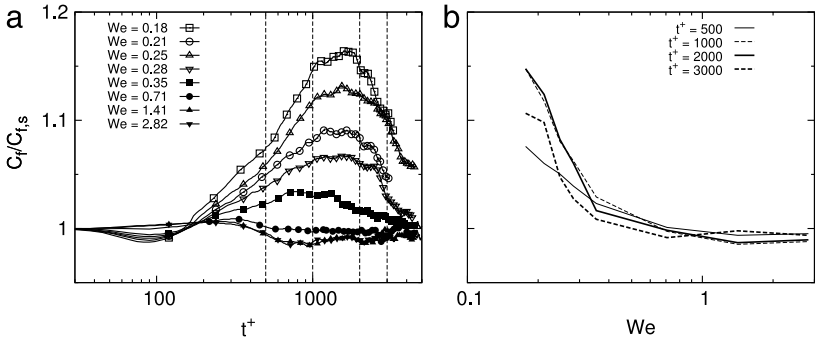

Fig. 4. Friction coefficient C_f normalized with the average friction coefficient measured in a single phase turbulent channel flow $C_{f,s}$. In panel (a), the time evolution of $C_f/C_{f,s}$ is reported; panel (b) depicts the dependence of the friction coefficient to the Weber number We at different times: $t^+ = 500, 1000, 2000, 3000$. Times are also shown as vertical lines in panel (a).

the total external surface of the droplet S that decreases in time. Moreover, due to the mid-channel segregation, droplets tend to move in a region of smaller velocity non-homogeneity, further reducing the velocity differences experienced by the droplets and emphasizing the modulation of C_f at $t^+ > 2000$. In Fig. 4(b) the friction coefficient is reported as function of We at four different times, confirming the presence of a quasi-steady state when $1000 \leq t^+ \leq 2000$. It is in any case clear that less deformable (or small We) droplets produce larger increments of C_f, as observed through time averaged statistics [8].

4. Conclusions

The segregation and wall-drag modifications produced by a swarm of large breaking and coalescing droplets dispersed in a fully turbulent channel flow have been investigated with a Phase Field Model. Concerning the dynamics of the dispersed phase, for small Weber ($We < 1$), coalescence dominates: in such regime, surface tension prevents fragmentation and a continuous decrement of the normalized number of droplets $n_d/n_{d,0}$ is observed until a universal asymptotic regime is reached. At large t^+, coalescence becomes a rare event because droplets are too distant to interact and $n_d/n_{d,0}$ stabilizes to a value that is We independent. On the contrary, for large Weber numbers ($We > 1$), $n_d/n_{d,0}$ does not decrease monotonically. Local turbulence causes droplets fragmentation if the diameter of a droplet is larger than a critical value and a dynamic equilibrium between coalescence and break-up is reached at large t^+. Although droplet/wall interaction is not prevented, the dispersed phase tend to accumulate at the center of the channel. This mechanism, qualitatively observed here, in agreement with previous numerical simulations [12], is influenced by We. The dynamics of the continuous (or carrier) phase is influenced

by the presence of the droplets: the friction coefficient of the flow is modified and its time evolution depends on the Weber number. Deformable droplets (higher We) are transported more effectively and the friction coefficient C_f is comparable with that measured in the single phase flow. Increasing the surface tension, C_f increases showing a time-dependent behavior: larger wall-drag is observed when an optimal balance between droplets total surface S and droplet average diameter $\langle d \rangle$ is reached.

Acknowledgments

CINECA Supercomputing Centre (Bologna, Italy) and ISCRA Computing Initiative are gratefully acknowledged for generous allowance of computer resources. Support from Regione Autonoma Friuli Venezia Giulia under grant PAR FSC 2007/2013 is gratefully acknowledged.

References

[1] R. Chella, J. Viñals, Mixing of a two-phase fluid by cavity flow, Phys. Rev. E 53 (4) (1996) 3832.
[2] D.M. Anderson, G.B. McFadden, A.A. Wheeler, Diffuse-interface methods in fluid mechanics, Annu. Rev. Fluid Mech. 30 (1) (1998) 139–165.
[3] A.G. Lamorgese, D. Molin, R. Mauri, Phase field approach to multiphase flow modeling, Milan J. Math. 79 (2) (2011) 597–642.
[4] F. Magaletti, F. Picano, M. Chinappi, L. Marino, C.M. Casciola, The sharp-interface limit of the Cahn–Hilliard/Navier–Stokes model for binary fluids, J. Fluid Mech. 714 (2013) 95–126.
[5] V.E. Badalassi, H.D. Ceniceros, S. Banerjee, Computation of multiphase systems with phase field models, J. Comput. Phys. 190 (2) (2003) 371–397.
[6] P. Yue, C. Zhou, J.J. Feng, Spontaneous shrinkage of drops and mass conservation in phase-field simulations, J. Comput. Phys. 223 (1) (2007) 1–9.
[7] L. Scarbolo, F. Bianco, A. Soldati, Coalescence and breakup of large droplets in turbulent channel flow, Phys. Fluids 27 (2015) 073302.
[8] L. Scarbolo, A. Soldati, Wall drag modification by large deformable droplets in turbulent channel flow, Comput. & Fluids 113 (2015) 87–92.
[9] G. Segre, A. Silberberg, Behaviour of macroscopic rigid spheres in Poiseuille flow Part 1. Determination of local concentration by statistical analysis of particle passages through crossed light beams, J. Fluid Mech. 14 (01) (1962) 115–135.
[10] G. Segre, A. Silberberg, Behaviour of macroscopic rigid spheres in Poiseuille flow Part 2. Experimental results and interpretation, J. Fluid Mech. 14 (01) (1962) 136–157.
[11] J.-P. Matas, J.F. Morris, É Guazzelli, Inertial migration of rigid spherical particles in Poiseuille flow, J. Fluid Mech. 515 (2004) 171–195.
[12] J. Lu, G. Tryggvason, Effect of bubble deformability in turbulent bubbly upflow in a vertical channel, Phys. Fluids (1994-present) 20 (4) (2008) 040701.
[13] S. Berti, G. Boffetta, M. Cencini, A. Vulpiani, Turbulence and coarsening in active and passive binary mixtures, Phys. Rev. Lett. 95 (2005) 224501. http://dx.doi.org/10.1103/PhysRevLett.95.224501.
URL: http://link.aps.org/doi/10.1103/PhysRevLett.95.224501.
[14] P. Perlekar, L. Biferale, M. Sbragaglia, S. Srivastava, F. Toschi, Droplet size distribution in homogeneous isotropic turbulence, Phys. Fluids 24 (6) (2012) 065101.
[15] D.M. Mitrinović, A.M. Tikhonov, M. Li, Z. Huang, M.L. Schlossman, Noncapillary-wave structure at the water-alkane interface, Phys. Rev. Lett. 85 (3) (2000) 582.
[16] A. Giacomello, S. Meloni, M. Chinappi, C.M. Casciola, Cassie–Baxter and Wenzel states on a nanostructured surface: Phase diagram, metastabilities, and transition mechanism by atomistic free energy calculations, Langmuir 28 (29) (2012) 10764–10772.
[17] J. Brackbill, D.B. Kothe, C. Zemach, A continuum method for modeling surface tension, J. Comput. Phys. 100 (2) (1992) 335–354.
[18] L. Scarbolo, A. Soldati, Turbulence modulation across the interface of a large deformable drop, J. Turbul. 14 (11) (2013) 27–43.
[19] P. Yue, J.J. Feng, C. Liu, J. Shen, A diffuse-interface method for simulating two-phase flows of complex fluids, J. Fluid Mech. 515 (1) (2004) 293–317.
[20] L. Scarbolo, D. Molin, P. Perlekar, M. Sbragaglia, A. Soldati, F. Toschi, Unified framework for a side-by-side comparison of different multicomponent algorithms: lattice Boltzmann vs. phase field model, J. Comput. Phys. 234 (2013) 263–279.
[21] J.O. Hinze, Fundamentals of the hydrodynamic mechanism of splitting in dispersion processes, AIChE J. 1 (1955) 289–295.
[22] A. Giusti, F. Lucci, A. Soldati, Influence of the lift force in direct numerical simulation of upward/downward turbulent channel flow laden with surfactant contaminated microbubbles, Chem. Eng. Sci. 60 (22) (2005) 6176–6187.
[23] D. Molin, C. Marchioli, A. Soldati, Turbulence modulation and microbubble dynamics in vertical channel flow, Int. J. Multiph. Flowv 42 (2012) 80–95.